OPTIMAL DESIGN AND SIMULATION OF DOUBLE-DISK FURROW OPENER FOR A PRECISION CORN PLANTER IN SALINE-ALKALI SOIL

1

盐碱地玉米精量播种机双圆盘开沟器优化设计与仿真

Zhihao DING¹¹, Dongwei WANG².³¹, Abouelnardar SALEM³¹, Yu TIAN³¹, Haoran BAl⁵¹¹, Farid Eltom ABDALLAH³.⁴¹, Ahmed F. El-SHAFIE³.⁴¹, Kai ZHAO¹¹, Yuanhao WANG¹¹

1) College of Mechanical and Electrical Engineering, Qingdao Agricultural University, Qingdao, Shandong/ China;

²⁾ Dongying QAU Saline-Alkali Land Efficient Agriculture Technology Industry Research Institute, Dongying / China; ³⁾ Yellow River Delta Intelligent Agricultural Machinery Equipment Industry Academy, Dongying / China;

4) Saline-Alkali Land Comprehensive Utilization Technology Innovation Center, Dongying / China

Tel: +8613999276706; E-mail: 839497789@gg.com

Corresponding author: Haoran BAI

DOI: https://doi.org/10.35633/inmateh-77-11

Keywords: Saline-alkali soil; Mechanical analysis; EDEM simulation, The optimal parameters

ABSTRACT

Traditional furrow openers used for corn planting in saline-alkali soils often face challenges such as high resistance, excessive soil disturbance, and unstable furrow depth, all of which negatively affect planting quality. This study presents an optimized design of a double-disk furrow opener for precision corn planting under saline-alkali conditions. The structure and working principle of the opener were described, and its force mechanism analyzed. Key structural parameters, including disk diameter, disk angle, and convergence angle of the disk points, were identified, with furrow resistance and furrow depth stability selected as evaluation indicators. Using a Box-Behnken design combined with EDEM simulation, the soil-machine interaction model was established, followed by variance analysis. The optimal parameters were determined as a disk diameter of 344 mm, disk angle of 12.9°, and convergence angle of 58.4°. Under these conditions, the operating resistance of the furrow opener was 370.234 N, and the furrow depth stability coefficient reached 93.87%. The results provide a theoretical basis for reducing furrow resistance and improving planting stability and efficiency in saline-alkali soils.

摘要

针对盐碱地玉米播种中,传统开沟器易出现工作阻力大、土壤扰动明显、开沟深度不稳定等问题,进而影响播种质量,本文对盐碱地玉米精量播种机双圆盘开沟器展开优化设计。首先,明确双圆盘开沟器的结构组成与工作原理,通过力学分析推导其受力机制;其次,确定关键参数圆盘直径、圆盘夹角、圆盘聚点位置,以开沟作业阻力和开沟深度稳定性系数为评价指标,采用 Box-Behnken 设计方法结合 EDEM 离散元仿真软件构建盐碱土于沟器互作模型,开展仿真试验并进行方差分析;确定最优结构参数组合为:圆盘直径 344mm、圆盘夹角 12.9°、圆盘聚点位置 58.4°,此时开沟器作业阻力为 370.234N,开沟深度稳定性系数为 93.87%。本研究为降低盐碱地播种作业阻力、提升播种稳定性和效率提供了理论依据。

INTRODUCTION

China has a large area, wide distribution, and diverse types of saline-alkali land (*Hu Y. et al., 2023*), which is widely distributed in multiple provinces and regions, mainly concentrated in the arid and semi-arid areas of the north and coastal areas. The soil has been severely affected by long-term salinization (*Wang D. et al., 2024*), resulting in severe compaction, which makes traditional trenchers face problems such as high operational resistance and unstable furrow depth during operation. Corn is a major economic crop worldwide, characterized by low planting costs and high yields (*Ding S.W. et al., 2022*). Sowing is a key measure in the corn planting process, and its quality directly affects crop yield. The seeding process of the corn precision sowing machine can be simply described as follows: within a continuous and stable seed furrow, with an extremely high probability, a complete seed is gently sown at each almost equal distance (*Li R. et al., 2017; Guo W., 2014*). This process has extremely high requirements for the furrow, ensuring the stability of the sowing depth, preventing the seeds from rolling at the bottom of the furrow, and avoiding damaging the seeds.

Therefore, designing and optimizing the double-disk furrow opener suitable for corn sowing operations in saline-alkali land is of great significance for improving the sowing stability, reducing the operational resistance, and minimizing soil disturbance.

Researchers from various countries have conducted extensive and in-depth research on the furrow opener of various types of seeders. *Dilwar et al., 2025,* conducted a study comparing the performance of three different furrow openers, namely concave disks, double disks, and punch hole, in the high-stubble rice-wheat rotation system (IRWRS). Through experiments, they found that the concave disk opener was the most suitable for no tillage sowing in IRWRS. *Tang et al., 2024,* used bionic design method to design a bionic furrow opener for paddy field fertilization according to the main physical characteristics of the badger claw, so as to improve the working efficiency of the furrow opener for paddy field fertilization. *Demshin et al., 2025,* analyzed the working process of the furrow opener disk cutter of the turf seeder and found the main problem: due to the impact load and high energy consumption, the torque transmitted by them was uneven. A damper safety device is proposed to solve this problem.

In order to improve the operational capability of the double-disk furrow opener in saline-alkali land, a 3D model of the double-disk furrow opener was first created in Solid Works software. Then, its mechanism of force receiving was explored through theoretical analysis, and the key parameters of the double-disk furrow opener are determined, including the diameter of the disk, the angle of the disk and the position of the disk accumulation point, and the range of their values was determined. The dynamic operation process of the double-disk furrow opener was simulated and analyzed using discrete element simulation software (EDEM) (Gao X. et al., 2024), and Box-Behnken response surface tests were conducted using Design-Expert experimental design software to ultimately determine the optimal combination of structural parameters for the double-disk furrow opener.

MATERIALS AND METHODS

Structure composition of double-disk furrow opener

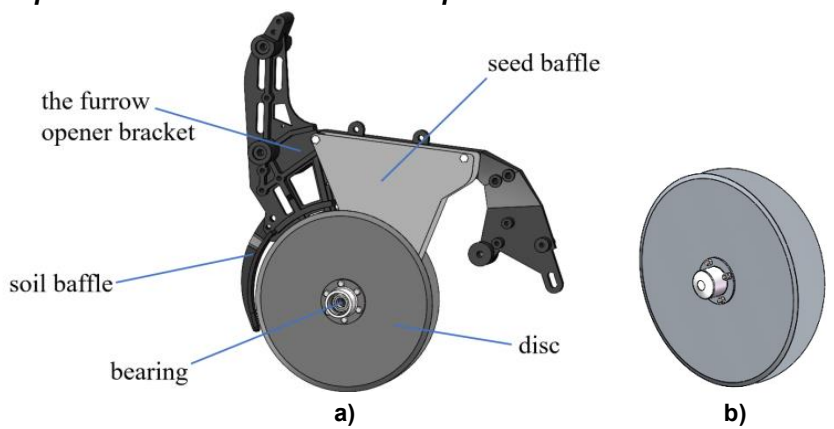


Fig. 1 - Schematic diagram of the structure of the double-disk furrow opener a) Overall structural schematic diagram; b) Simplified structural schematic diagram

The double-disk furrow opener is symmetrically mounted on both sides of the furrow opener bracket using two disks of identical size. The disks meet at a specific angle at the cutting edge (*Zhao Y. et al., 2018*). Between the two disks is a seed baffle that serves as a seed guide, which is fixed to the furrow opener bracket. A soil baffle is installed in front of the disks, and the structure is shown in Fig. 1a. To facilitate subsequent theoretical analysis, structural design, and simulation experiments, the model was simplified as shown in Fig.1b.

Working principle of double-disk furrow opener

When working in the field, the double-disk furrow opener mainly relies on its own weight and the weight of the seeder body to exert downward pressure to penetrate and break the soil. The double-disk furrow opener enters the soil and rotates forward with the disk accumulation point as the breaking point to cut the soil. Because there is a certain angle between the two disks, the two disks squeeze the soil on both sides and open the seed furrow in the process of advancing (*Che J et al., 2018*). Driven by the seeder, the furrow opener rotates forward, and the width between the disks gradually increases, forming a suitable width of the seed furrow.

Mechanical analysis of soil cutting by the double-disk furrow opener

The cutting edges of the double-disk furrow opener are in the form of arcs. In the working state, the cutting edges that perform the cutting function are the arc-shaped edges formed by the intersection area of the two disks (Ahmad D et al., 2004). Due to the fact that each point on the arc changes position as the disks rotate continuously, the depth of each point in the soil is also different. Therefore, in order to more accurately calculate the force during the cutting process, the cutting edges of the disks can be projected onto a plane perpendicular to the direction of movement. This projected area can be divided into multiple small units. By analyzing the force received by each unit and integrating them one by one, the force state during the entire furrowing process can be obtained. This approach not only simplifies the calculation process of force but also makes the analysis of the force distribution and depth changes more precise and accurate.

The double-disk furrow opener causes damage to the soil structure during its movement, leading to soil failure. According to the passive soil pressure theory model, when the soil is disturbed, it will undergo shear failure at a certain angle. The angle between this failure surface and the horizontal plane is denoted as α, and y represents the internal friction angle of the soil. This failure results in soil sliding above the failure surface, eventually forming a soil wedge structure. For ease of analysis, each small unit within the projection area can be equivalently regarded as a plane. At this time, each plane forms a soil wedge structure (as shown in Figure 3). Based on this assumption, the static analysis method can be used to analyze the force on the soil wedge structure, thereby further deriving the resultant force and distribution pattern of each small unit on the entire projection surface.

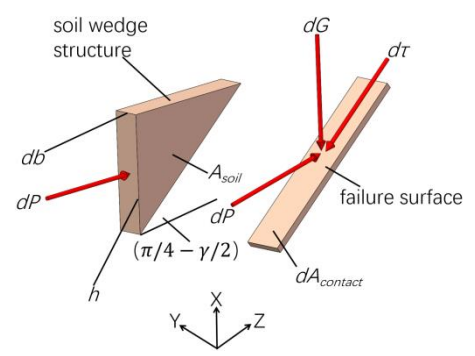


Fig. 3 - Schematic diagram of mechanical analysis of soil cutting by the double-disk furrow opener

The force analysis of the soil wedge structure shows that it is subjected to three forces (Ahmadi I. et al., 2016): the gravitational force of the soil wedge dG, the shear resistance between soil particles $d\tau$, and the cutting force of the disk dP. According to the force equilibrium condition, at the moment of soil failure, the following equations must be satisfied:

$$\alpha = \left(\frac{\pi}{4} - \frac{\gamma}{2}\right) \tag{1}$$

$$dP\cos\alpha - dG\sin\alpha = d\tau \tag{2}$$

Among these forces, the gravitational force dG acting on the soil wedge satisfies the following equations:

$$dG = \rho_{soil} \times g \times dV_{soil} = \rho_{soil} \times g \times db \times A_{soil}$$
 (3)

$$dG = \rho_{soil} \times g \times dV_{soil} = \rho_{soil} \times g \times db \times A_{soil}$$

$$A_{soil} = \frac{h^2}{2 \tan \alpha}$$
(4)

where: ρ_{soil} is the soil density, [kg/m³]; g is the gravitational acceleration, [m/s²]; dV_{soil} is the volume of the soil wedge, [mm³]; A_{soil} is the lateral surface area of the soil wedge, [mm²]; db is the width of the soil wedge, [mm]; h is the height of the soil wedge, [mm].

The shear resistance $d\tau$ satisfies the following equations:

$$d\tau = c \times dA_{contact} + dF \times tan \gamma \tag{5}$$

$$dF = dP \sin \alpha + dG \cos \alpha \tag{6}$$

$$dA_{contact} = \frac{db \times h}{\sin \alpha} \tag{7}$$

where:

c is the soil cohesion; $dA_{contact}$ is the area of contact between the disk and the soil, [mm²]; dF is the normal positive pressure on the failure surface, [N].

The combination of equation (4) to (8) yields:

$$d\tau = c \frac{db \times h}{\sin \alpha} + [dP \sin \alpha + \rho_{soil} \times g \times db \times A_{soil} \cos \alpha] \tan \gamma \tag{8}$$
 By combining equation (9) and equation (3), it can be derived that:

$$dP\cos\alpha - dG\sin\alpha = c\frac{db\times h}{\sin\alpha} + [dP\sin\alpha + \rho_{soil}\times g\times db\times A_{soil}\cos\alpha]\tan\gamma \tag{9}$$

Simplifying the above equation yields the following result:
$$dP = c \frac{db \times h}{\sin \alpha (\cos \alpha - \sin \alpha)} + \frac{\rho_{soil} \times g \times db \times A_{soil} (\sin \alpha + \cos \alpha \tan \gamma)}{\cos \alpha - \sin \alpha \tan \gamma}$$
 (10)

Mechanical analysis of the soil displacement process

During the operation of the double-disk furrow opener, the disks maintain a uniform forward motion, continuously cutting into the soil, while the soil moves forward along the surface of the disks. The forward movement of the soil is continuous and uninterrupted. The forces acting on the soil along the disk surface can be determined using the principle of impulse and momentum (Beer F. P., 1965). First, the soil adjacent to the disk surface is defined as a control volume element. According to the impulse-momentum principle, the impulse generated by the resultant external force acting on this element is equal to the change in momentum of the soil moving along the surface of the control volume.

From a physical standpoint, a stable particle flow state exists during the interaction between the disk and the soil. In this state, the final momentum of the soil particles leaving the control volume element is equal to the vector sum of the initial momentum of the soil particles entering the control volume element and the impulse produced by the resultant external force over the corresponding period of action. It is important to note that the change in momentum involves not only variations in the speed of the soil particles but also adjustments in their direction of motion, as shown in Fig. 4.

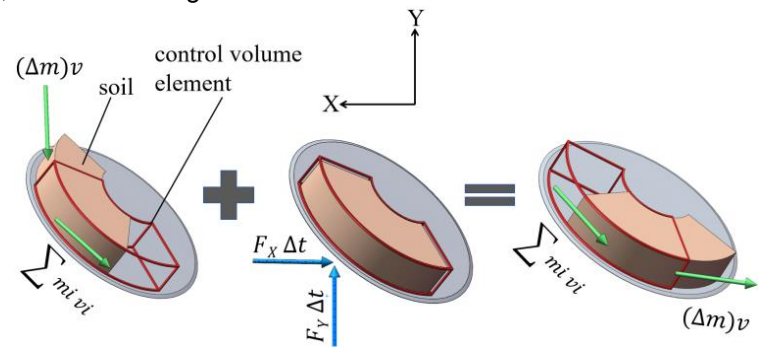


Fig. 4 - Schematic diagram of mechanical analysis of the soil displacement process

According to the principle of momentum impulse, based on the working conditions of the soil within the control volume element shown in the diagram, the following equations can be derived.

Force analysis in the Y-direction leads to the following equation:

$$-(\Delta m)v + F_V \Delta t = -(\Delta m)v \cos \eta \tag{11}$$

Force analysis in the X-direction leads to the following equations:

$$F_{\mathbf{x}}\Delta t = (\Delta m)v\sin\eta\tag{12}$$

$$\Delta m = \rho_{soil} A_X v \Delta t \tag{13}$$

$$A_X = A\cos\theta\cos\delta\tag{14}$$

where: Δt is the action time, [s]; Δm is the mass of the soil that flows through during the action time Δt , [kg]; v is the velocity of the soil relative to the disk, [m/s]; η is the angle between the displaced soil and the horizontal plane, [°]; θ is the angle of inclination of the disk, [°]; δ is the tilt angle of the disk, [°]; A_X is the contact area between the control volume element and the disk in the X-direction, [mm²]; A is the contact area between the control volume element and the disk, [mm²].

By combining equation (12) and equation (15), it can be derived that:

$$F_Y = A\cos\theta\cos\delta\rho_{soil}v^2(1-\cos\eta) \tag{15}$$

$$F_X = A\cos\theta\cos\delta\rho_{soil}v^2\sin\eta \tag{16}$$

According to Newton's third law, the action force is equal in magnitude and opposite in direction to the reaction force. The pressure N exerted on the surface of the disk by the soil is equal to the force F_X exerted by the disk on the soil in the X-direction; the resistance F_{dX} acting on the disk by the soil is equal to the force F_Y exerted by the disk on the soil in the Y-direction.

Analysis of the slip resistance between the disk and the soil

The slip resistance generated during the interaction between the disk and the soil can be divided into two parts. The first part is the slip resistance generated between the surface of the disk and the soil during the rotating forward process of the disk. This resistance mainly comes from the relative motion between the disk surface and the soil particles, manifested as the resistance exerted by the soil particles on the disk surface. The second part is the frictional force between the disk edge and the soil, which mainly occurs during the process of the disk edge cutting into the soil.

During the interaction between the soil and the disk surface, in addition to the frictional force, there is also the adhesion force generated due to the physicochemical properties of the soil. This adhesion force is not only related to the soil's moisture, particle state, and density but is also influenced by changes in the internal structure of the soil. Variations in the adhesion force can cause fluctuations in the normal load on the contact interface, which in turn affects the slip resistance between the disk and the soil. Therefore, the slip resistance acting on the disk surface can be divided into two components: frictional force and adhesion force (*Gill W. R. et al., 1967*). The calculation formula is as follows:

$$f_1 = \mu N + \mu F_a A_W = \mu F_x + \mu F_a A_W = \mu A \cos \theta \cos \delta \rho_{soil} v^2 \sin \eta + \mu F_a A_W$$
 (17) where: f_I is the slip resistance exerted on the surface of the disk, [N]; μ is the coefficient of kinetic friction between the soil and the disk; F_a is the adhesive load caused by the water film, [Pa]; A_W is the area of the adsorbed water film, [mm²].

The normal pressure exerted on the edge during soil cutting is the supporting force from the soil on the entire the double-disk furrow opener, and the magnitude of the force is the weight of the entire double-disk furrow opener (including the furrow opener bracket). The slip resistance exerted at the edge is as shown in the following formula:

$$f_2 = \mu g m_{total} = \mu g (m_{disc} + m_{bracket}) \tag{18}$$

where: f_2 is the slip resistance exerted at the edge, [N]; m_{disk} is the mass of the disk, [kg]; $m_{bracket}$ is the mass of the furrow opener bracket, [kg].

The total slip resistance exerted on the disk is as follows:

$$f_{total} = f_1 + f_2 = \mu A \cos\theta \cos\delta\rho_{soil} v^2 \sin\eta + \mu F_a A_W + \mu g(m_{disc} + m_{bracke})$$
 (19)

Structural design of the double-disk furrow opener

First, regarding the design of the disk, the disk diameter should not be too small, as a small diameter can cause poor coordination between the disks, leading to problems such as jamming, increased resistance, and reduced operational quality. Conversely, the diameter should not be too large, as an oversized disk can produce an excessively wide furrow, poor seed furrow shape, unstable sowing depth, excessive soil disturbance, and rapid moisture loss (*Che J. et al., 2018*). Based on the agronomic requirements for corn planting and the above mechanical analysis, the recommended range for the disk diameter *D* is 320–400 mm.

During the operation of the furrow opener, the included angle φ between the disks should be designed appropriately (*Zhao Y. et al., 2018*). A smaller included angle results in lower operating resistance for the furrow opener. However, if the angle is too small, the space between the two disks becomes insufficient to accommodate the seed baffle, and the seed furrow becomes too narrow. Conversely, if the included angle is too large, the operational resistance of the furrow opener increases, the seed furrow becomes wider, the amount of soil return rises, and soil disturbance intensifies, leading to more floating soil at the bottom of the seed furrow and poorer sowing depth stability (*Malasli et al., 2019*). Therefore, based on the above theoretical and mechanical analysis, the disk angle φ is typically designed within the range of 10° – 20° .

The two disks of the double-disk furrow opener intersect at the cutting edge at a single point, known as the disk point of convergence m. The position of this point is represented by the angle β , as shown in Figure 5. If the β angle is too large, the point m will be positioned too high, resulting in a wider seed furrow and causing the soil in the middle of the furrow to rise, leading to poorer furrow stability. If the β angle is too small, the point m will be positioned too low, allowing soil to fall into the gap above the disk point of convergence, causing uneven sowing depth, disk soil clogging, and faster bearing wear (Li D., 2021).

Table 1

Based on the above theoretical and mechanical analysis, the typical range for this angle β is between 55° and 75° (Chinese Academy of Agricultural Mechanization Sciences, 2007).

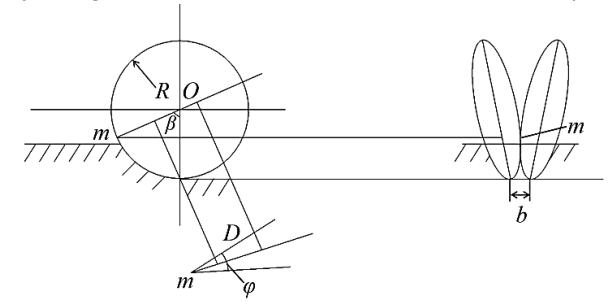


Fig. 5 - Schematic diagram of the position of the disk convergence point

The width of the seed furrow opened by the furrow opener is determined by the disk diameter D, disk angle φ , and the position of the disk point of convergence m. According to the literature, the calculation formula is as follows:

$$b = D(1 - \cos \beta) \sin \frac{\varphi}{2} \tag{20}$$

where: b is the seed furrow width, [mm]; D is the disk diameter, [mm]; β is the angle of the point of convergence, [°]; φ is the disk angle, [°].

Establishing the EDEM simulation model

Save the completed the double-disk furrow opener 3D models in Solid Works software as STL files and import them into EDEM software. Using EDEM software, create a soil bin simulation model with dimensions of 1500mm in length, 500mm in width, and 200mm in height, then produce 172000 soil particle models with a bonding radius of 5mm within the model. To simulate the fragmentation of the soil, select the Hertz Mindlin with bonding model. And set the forward speed to 1.5 m/s and the sowing depth to 40 mm according to the agronomic requirements for corn planting, as shown in Figure 6(*Jiang B et al., 2025*). Referencing the research findings from relevant literature on saline-alkali soil, the relevant parameters for each material are provided in Table 1(*Wang D. et al., 2024; Xu N. et al., 2025*).

The completed 3D models of the double-disk furrow opener were exported from SolidWorks as STL files and imported into EDEM. In EDEM, a soil-bin simulation model was created with dimensions of 1500 mm (length) × 500 mm (width) × 200 mm (height). Within this domain, 172000 soil particles were generated using a bonding radius of 5 mm. To simulate soil fragmentation, the Hertz–Mindlin with bonding contact model was selected. The forward speed was set to 1.5 m/s and the sowing depth to 40 mm, in accordance with agronomic requirements for corn planting, as shown in Fig. 6 (*Jiang B. et al., 2025*). Material parameters for each component were assigned based on studies of saline–alkali soils; the corresponding values are listed in Table 1 (*Wang D. et al., 2024; Xu N. et al., 2025*).

Relevant parameters of discrete element simulation model

Parameters	Numerical Value
Density of steel [kg·m ⁻³]	7865
Shear modulus of steel [Pa]	7.9x10 ¹⁰
Poisson's ratio of steel	0.3
Saline-alkali soil particle density [kg·m ⁻³]	2290
Poisson's ratio of saline-alkali soil	0.32
Saline-alkali soil shear modulus [Pa]	1 x10 ⁶
Soil-soil static friction coefficient	0.546
Soil-soil rolling friction coefficient	0.15
Soil-soil restitution coefficient	0.358
Soil-steel static friction coefficient	0.5
Soil-steel rolling friction coefficient	0.17
Soil-steel restitution coefficient	0.3
Soil normal bonding stiffness [N·m ⁻³]	5x10 ⁸
Soil tangential bonding stiffness [N·m ⁻³]	5x10 ⁸
Soil critical normal stress [Pa]	3x10 ⁶
Soil critical tangential stress [Pa]	3x10 ⁶
Soil particle bonding radius [mm]	5.16

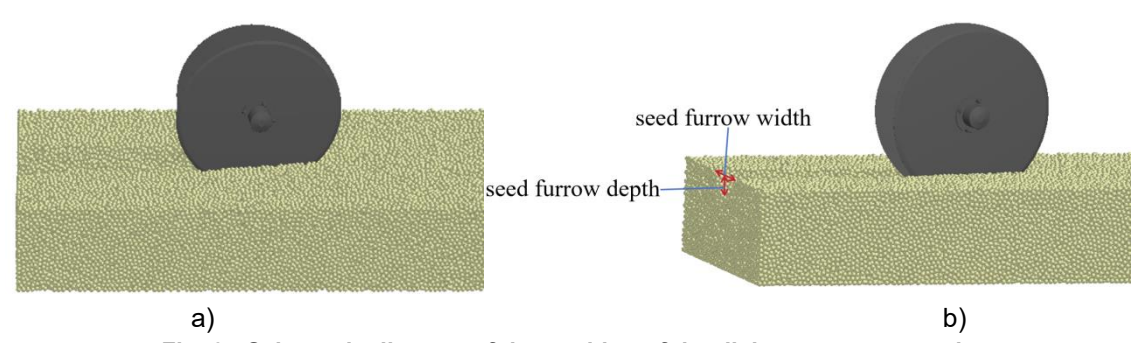


Fig. 6 - Schematic diagram of the position of the disk convergence point
a) Soil and double-disk furrow opener simulation model; b) Schematic diagram of seed furrow

RESULTS

Box-Behnken Design Simulation tests

Based on the mechanical and structural theoretical analysis of the double-disk furrow opener, it can be concluded that the parameters that play a decisive role in the furrowing operation are the disk diameter (D), disk angle (φ), and the angle of the disk point of convergence (β). These three parameters were selected as experimental factors, and their value ranges were determined. The furrow resistance (Y_1) and the stability coefficient of furrow depth (Y_2) were used as evaluation indicators. A three-factor, three-level Box-Behnken design in the Design Expert software was used to study the relationship between the experimental factors and the evaluation indicators, further determining the optimal structural parameter combination for the double-disk furrow opener. The factors coding situation is shown in Table 2, and the experimental design scheme and results are shown in Table 3.

Experimental factors coding table

Table 2

		•		
	Encodings —		Factors	
		D [mm]	φ["]	β ["]
	-1	320	10	55
	0	360	15	65
	1	400	20	75

Experimental design scheme and results

Table 3

Serial	Factors			Evaluation indicators		
Number	D [mm]	φ [°]	β[°]	Y ₁ [N]	Y ₂ [%]	
1	400	10	65	412.682	85.19	
2	400	15	55	420.050	87.26	
3	360	15	65	409.250	93.46	
4	400	20	65	489.189	81.53	
5	320	10	65	398.176	89.53	
6	360	10	75	458.736	91.55	
7	320	20	65	442.649	89.21	
8	360	15	65	395.346	93.41	
9	360	15	65	387.562	92.35	
10	360	15	65	380.925	93.56	
11	360	10	55	393.590	92.66	
12	320	15	75	458.074	90.25	
13	320	15	55	373.485	91.64	
14	360	15	65	383.027	92.83	
15	400	15	75	496.598	83.67	
16	360	20	55	445.621	91.47	
17	360	20	75	494.782	91.05	

In calculating the furrow depth stability coefficient, the equidistant sampling method is used. Five measurement points are taken at equal intervals along the travel direction. The average furrow depth and standard deviation are calculated to obtain the furrow depth stability coefficient, as shown in the following formula:

$$\bar{h} = \frac{\sum_{i=1}^{n} h_i}{N_{point}} \tag{21}$$

$$\bar{h} = \frac{\sum_{i=1}^{n} h_i}{N_{point}}$$

$$S = \sqrt{\frac{\sum_{i=1}^{n} (h_i - \bar{h})^2}{N_{point} - 1}}$$
(21)

$$U = 1 - \frac{s}{h} \times 100\% \tag{23}$$

where:

 \bar{h} is the average furrow depth, [mm]; h_i is the furrow depth value at the *i*-th measurement point, [mm]; N_{point} is the number of selected measurement points; S is the standard deviation of the furrow depth, [mm]; U is the furrow depth stability coefficient, [%].

Table 4 Analysis of variance in the simulation test of the furrow resistance

Model 26831.17 9 2981.24 20.66 0 D 2669.42 1 2669.42 18.50 0 φ 5463.12 1 5463.12 37.85 0 β 9483.67 1 9483.67 65.71 Dφ 256.55 1 256.55 1.78 0 Dβ 16.16 1 16.16 0.1120 0 φβ 63.88 1 63.88 0.4426 0 D² 1168.75 1 1168.75 8.10 0 φ² 3252.00 1 3252.00 22.53 0 β² 3582.46 1 3582.46 24.82 0 Residual 1010.32 7 144.33 - Lack of Fit 481.72 3 160.57 1.22 0 Pure Error 528.60 4 132.15 - -		•				
$\begin{array}{cccccccccccccccccccccccccccccccccccc$	Source	Sum of Squares	df	Mean Square	F-value	P-value
	Model	26831.17	9	2981.24	20.66	0.0003
β 9483.67 1 9483.67 65.71 < $ρ$	D	2669.42	1	2669.42	18.50	0.0036
$\begin{array}{c ccccccccccccccccccccccccccccccccccc$	φ	5463.12	1	5463.12	37.85	0.0005
$\begin{array}{c ccccccccccccccccccccccccccccccccccc$	β	9483.67	1	9483.67	65.71	< 0.0001
$\begin{array}{c ccccccccccccccccccccccccccccccccccc$	Dφ	256.55	1	256.55	1.78	0.2242
$\begin{array}{cccccccccccccccccccccccccccccccccccc$	Dβ	16.16	1	16.16	0.1120	0.7477
$\begin{array}{c ccccccccccccccccccccccccccccccccccc$	φβ	63.88	1	63.88	0.4426	0.5272
$\begin{array}{c ccccccccccccccccccccccccccccccccccc$	D^2	1168.75	1	1168.75	8.10	0.0248
Residual 1010.32 7 144.33 - Lack of Fit 481.72 3 160.57 1.22 0 Pure Error 528.60 4 132.15 -	ϕ^2	3252.00	1	3252.00	22.53	0.0021
Lack of Fit 481.72 3 160.57 1.22 C Pure Error 528.60 4 132.15 -	β^2	3582.46	1	3582.46	24.82	0.0016
Pure Error 528.60 4 132.15 -	Residual	1010.32	7	144.33	-	-
	Lack of Fit	481.72	3	160.57	1.22	0.4124
Cor Total 27841 49 16	Pure Error	528.60	4	132.15	-	-
2011000	Cor Total	27841.49	16	-	-	-

Table 5 Analysis of variance in the simulation test of the furrow depth stability coefficient

Source	Sum of Squares	df	Mean Square	F-value	P-value
Model	205.22	9	22.80	47.59	< 0.0001
D	66.01	1	66.01	137.76	< 0.0001
φ	4.02	1	4.02	8.39	0.0231
β	5.30	1	5.30	11.06	0.0127
Dφ	2.79	1	2.79	5.82	0.0466
Dβ	1.21	1	1.21	2.53	0.1561
φβ	0.1190	1	0.1190	0.2484	0.6335
D^2	110.26	1	110.26	230.11	< 0.0001
ϕ^2	11.32	1	11.32	23.63	0.0018
β ²	0.1688	1	0.1688	0.3524	0.5714
Residual	3.35	7	0.4792	-	-
Lack of Fit	2.28	3	0.7613	2.85	0.1692
Pure Error	1.07	4	0.2676	-	-
Cor Total	208.57	16	-	-	-

Through the analysis of variance (ANOVA) on the experimental design results, as shown in Table 4 and Table 5, it can be concluded that the disk diameter (D), disk angle (φ) , and the angle of the disk point of convergence (β) have a highly significant impact on the furrow resistance and the furrow depth stability coefficient. Based on the ANOVA, regression equations were established between D, φ , and β and the furrow resistance (Y_1) as well as the furrow depth stability coefficient (Y_2) , as shown in the following formulas. To more intuitively visualize the interactive effects of D, φ and β on Y_1 and Y_2 , Design-Expert software was used to generate response surface plots, as shown in Figures 7 and 8 (*He J et al.*, 2025).

$$Y_1 = +391.22 + 18.27D + 26.13\varphi + 34.43\beta + 8.01D\varphi - 2.01D\beta - 4.00\varphi\beta + 16.66D^2 + 27.79\varphi^2 + 29.17\beta^2$$
 (24)

$$Y_2 = +93.12 - 2.87D - 0.7088\varphi - 0.8138\beta - 0.8350D\varphi - 0.5500D\beta + 0.1725\varphi\beta - 5.12D^2 - 1.64\varphi^2 + 0.2003\beta^2$$
 (25)

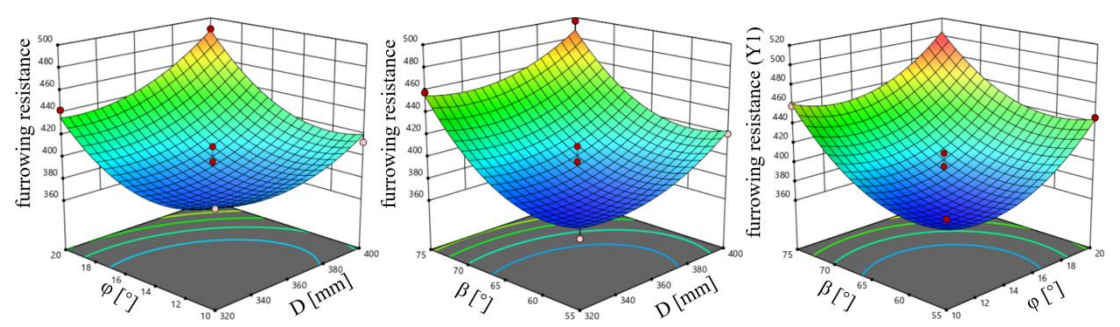


Fig. 7 - Response surface for the interactive influence of various factors on the furrow resistance

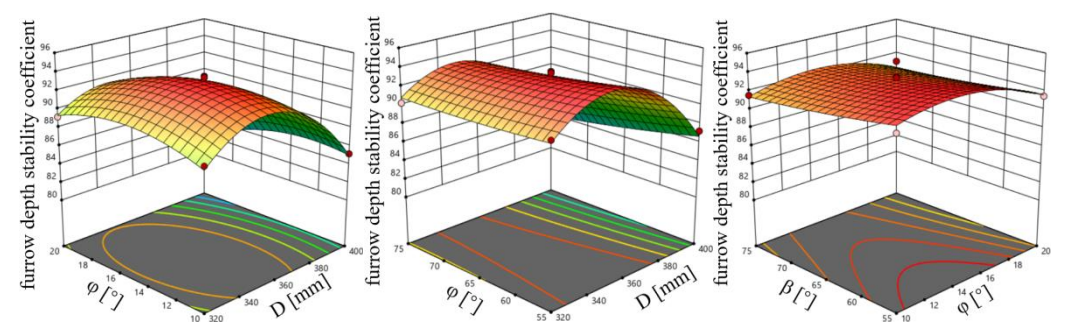


Fig. 7 - Response surface for the interactive influence of various factors on the furrow depth stability coefficient

To obtain the optimal parameter combination for D, φ , and β , the optimization module of Design-Expert was used. The objective function and constraint conditions are as followed:

$$\begin{cases}
\min Y_{1}(X_{1}, X_{2}, X_{3}) \\
\max Y_{2}(X_{1}, X_{2}, X_{3}) \\
320mm \le X_{1} \le 400mm \\
10^{\circ} \le X_{2} \le 20^{\circ} \\
55^{\circ} \le X_{3} \le 75^{\circ}
\end{cases} \tag{23}$$

After data processing, the optimal structural parameter combination was determined to be *D* is 344 mm, φ is 12.9°, and β is 58.4°. At this configuration, Y_1 is 370.234 N, and Y_2 is 93.87%.

CONCLUSIONS

First, considering the characteristics of saline-alkali soil and the agronomic requirements for corn planting, the double-disk furrow opener was optimized. The 3D model of the double-disk furrow opener was created using SolidWorks software, and its working principle was analyzed. A detailed mechanical analysis was then carried out for the entire furrowing process, including soil cutting by the double-disk furrow opener, the forces generated by soil displacement along the disk surface, and the slip resistance between the disk and the soil. This mechanical analysis provided a clearer understanding of the soil-tool interaction, offering a theoretical basis for subsequent parameter optimization.

Subsequently, through theoretical analysis, the key structural parameters and their ranges were determined. The disk diameter, disk angle, and convergence angle of the disk points were selected as experimental factors, with furrow resistance and furrow depth stability coefficient were chosen as evaluation indicators. The Box-Behnken design module in Design-Expert software was used to generate the experimental design, and simulation experiments were performed using EDEM software. Finally, variance analysis and predictive modeling of the simulation results were conducted in Design-Expert. The optimal parameter combination was found to be the disk diameter (D) = 344 mm, the disk angle (φ) = 12.9°, and convergence angle of the disk points (β) = 58.4°. Under these conditions, the furrow resistance (Y_1) was 370.234 N, and the furrow depth stability coefficient (Y_2) reached 93.87%.

ACKNOWLEDGEMENT

This research is supported by the National Key Research and Development Program of China (Project no. 2023YFD2001400); Innovative Key Technologies and Industrialization of Combined Equipment for Cultivation and Sowing in Saline-Alkaline Land (2024CGZH14); National Key R&D Program of China (Project no.2022YFE0125800); Creation of Key Intelligent Seeding Equipment for Saline-Alkaline Land (WSR2024092); Research and Application of Intelligent Breeding Equipment for Crops (2024LZGC004).

REFERENCES

- [1] Ahmad D, Amran F A. (2004). Energy prediction model for disk plow combined with a rotary blade in wet clay soil [J]. *International Journal of Engineering and Technology*, 1(2): 102-114.
- [2] Ahmadi I. (2016). Development and assessment of a draft force calculator for disk plow using the laws of classical mechanics [J]. *Soil & Tillage Research*, 163:32-40.
- [3] Beer F P. (1965). Vector Mechanics for Engineers: Statics and Dynamics [M]. McGraw Hill, U.S.
- [4] Chinese Academy of Agricultural Mechanization Sciences. (2007). Agricultural Machinery Design (Volume 1) (农业机械设计(上册)). China Agricultural Science and Technology Press, Beijing/China..
- [5] Che J., Yu L., Li Q. (2011). Design and Experimental Research of Double-disk Type No-tillage Wheat Seeding Machine (双圆盘式小麦免耕播种机设计与试验研究). *Journal of Shandong University of Technology (Natural Science Edition)*, 25(06), 25-28.
- [6] Ding S.W., Sun Z.Z., Li Q.L. (2022). Improving the level of agricultural mechanization and promoting the sustainable development of agriculture (提高农业机械化水平,促进农业可持续发展) [J]. *Contemporary Agricultural Machinery*, (10): 39-41.
- [7] Demshin Sergej, Saitov Viktor, Simonov Maksim, Zyryanov Dmitrij Demshin Konstantin. (2025). Determination of the parameters of the damper device of the milling furrow opener of the sod seeder. *E3S Web of Conferences*, 623,04027-04027.
- [8] Dilwar Singh Parihar, Mahesh Kumar Narang, Baldev Dogra, Amit Kumar, Dattatray G. Bhalekar.(2025). Performance evaluation of furrow openers for conservation tillage in intensive rice—wheat system. *Vegetos*, (prepublish), 1-11.
- [9] Gill W.R., Vanden Berg G.E. (1967). Soil Dynamics In Tillage And Traction. *Agricultural Research Service, U.S. Dept. of Agriculture*, Washington/U.S.
- [10] Guo W. (2014). Design and Experimental Research of the Furrow Maker for Precision Planters (精密播种机开沟器的设计与试验研究). *Agricultural Mechanization Research*, 36(07), 160-164.
- [11] Gao X., Yang W., Li J., Dai Y., Wang X., Chi Peng. (2024). Simulation Analysis of the Double-disk Furrowing Machine for Wheat Fields Based on EDEM (基于 EDEM 的小麦小区双圆盘开沟器仿真分析). *Agricultural Mechanization Research*, 46(12), 162-166+173.

- [12] Hu Y., Yang F., Yang N., Jia W., Cui Y. (2023).Analysis of Saline-Ash Soil Resources and Research Prospects on Their Utilization (盐碱地资源分析及利用研究展望). *Soil Bulletin*, 54(02), 489-494.
- [13] He J., He J. (2025). Optimization and Experiment of Key Components of Corn No-Till Seeding Machine Based on Response Surface Analysis Method (基于响应面分析法玉米免耕播种机关键部件优化及试验). *Agricultural Mechanization Research*, 47(05), 158-164.
- [14] Jiang B., Cai J., Chen X., Liu J., Xiao L., Lin J., Chen Y.(2025). Study on the Interactions Process of Coupled Model of Furrow Opener–Soil–Pot Seedling Based on Discrete Approach. Agriculture, 15(11), 1206-1206.
- [15] Li R., Yi S., Zhao B., Li Y., Yang L. (2017). Design of the 2BJM-12 Air-Suction Type No-Till Precision Sowing Machine (2BJM-12 型气吸式免耕精密播种机设计). *Agricultural Mechanization Research*, 39(12), 63-67.
- [16] Li D. (2021). Optimization of processing technology for the double-disk furrow opener of the seeder (播种机双圆盘开沟器加工工艺优化). *Agricultural Engineering*, 11(04), 25-28.
- [17] Malasli Z.M., Çelik Ahmet (2019). Disk angle and tilt angle effects on forces acting on a single-disk type no-till seeder opener [J]. *Soil & Tillage Research*. 194(2), 104304. DOI: 10.1016/j.still.2019.104304
- [18] Tang Z., Zeng Z., Wu S., Fu D., He J., Cai Y., Qi L. (2024). Optimizing soil resistance and disturbance of bionic furrow opener for paddy field based on badger claw using the CFD-DEM method. *Computers and Electronics in Agriculture*, 227(P1), 109549-109549.
- [19] Wang D., Lu T., Zhao Z., Shang S., Zheng S., Liu J. (2024). Simulation Parameter Calibration Method for the Cultivation Layer Soil in Coastal Saline-Ashy Land (滨海盐碱地耕作层土壤离散元仿真参数标定方法). *Journal of Agricultural Machinery Science*, 55(11), 240-249.
- [20] Xu N., Xin Z., Yuan J., Gao Z., Tian Y., Xia, C., Liu X., Wang D. (2025). Calibration of Discrete Element Simulation Parameters and Model Construction for the Interaction Between Coastal Saline Alkali Soil and Soil-Engaging Components. *Agriculture*, 15(1), 7.
- [21] Zhao Y., Wang Y., Yu D. (2018).Research on the Influence of Structural Parameters of Double-disk Furrowing Machine on Operating Performance (双圆盘开沟器结构参数对作业性能影响研究). *Agricultural Mechanization Research*, 40(11), 44-50.